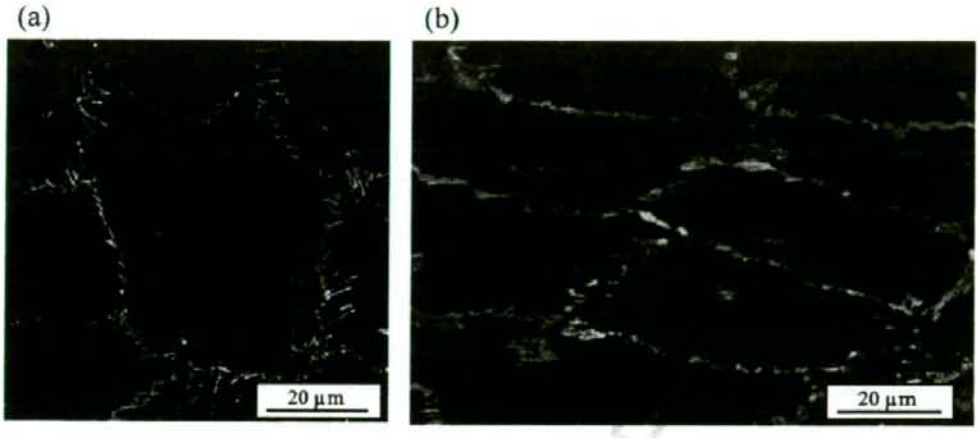

Fig. 1. Typical morphological changes of human umbilical vein endothelial cells in response to fluid shear stress. (a) Static condition: red are actin filaments; green is VE-cadherin. (b) Cells elongate in the flow direction (from the left to right) after exposure to shear. (The colors are visible in the online version of the article.)

fiber (Fig. 1) in concert with focal adhesion remodeling are regulated by a signaling cascade involving the RhoA small GTPase [5,28,50]. Previous studies have demonstrated that, in addition to the activations of Rho and its downstream effectors Rho-kinase and mDia, mechanical stress by itself affects the stress fiber remodeling [20,31]. Stress fibers in non-motile cells are contracted in an ATP-dependent manner while keeping a constant length between fixed focal adhesions (i.e., isometric contraction). Hence, tensions are always present in stress fibers even in the absence of external loading such as fluid shear stress and substrate stretch. The isometric contraction allows extracellular matrix (ECM) assembly and resultant wound healing [16,48,64]. Recent studies have demonstrated that changes in the isometric contraction caused by external loadings, such as alteration in tension or stress level, affect the molecular dynamics responsible for the contraction, and as a result elicit mechanosensitive responses of stress fibers.

Biomechanical properties of stress fibers including contractile behavior and resistance to mechanical loading would therefore have an important influence on their mechanosensing process. In this review, after emphasizing the differences in stress fibers between motile and non-motile cells, we discuss the biomechanical properties and behaviors of the stress fibers of non-motile cells based on reported measurement data and analyses.

2. Structural differences of stress fibers between motile and non-motile cells

To understand the contraction mechanism of stress fibers, knowledge of the actin filament polarity inside of the stress fiber is the most basic because it provides the direction of myosin motor movement along actin filaments (i.e., from pointed or minus end to barbed or plus end). Cramer et al. [7] detected the polarity by electron microscopy using myosin subfragment-1 head decoration. Spatial orientations of individual actin filaments along stress fibers were different between motile and non-motile cells, though the same term "stress fiber" is often used to refer to such structurally and functionally different actin bundles. Characteristics of the structures are schematically shown in Fig. 2 based on Cramer's

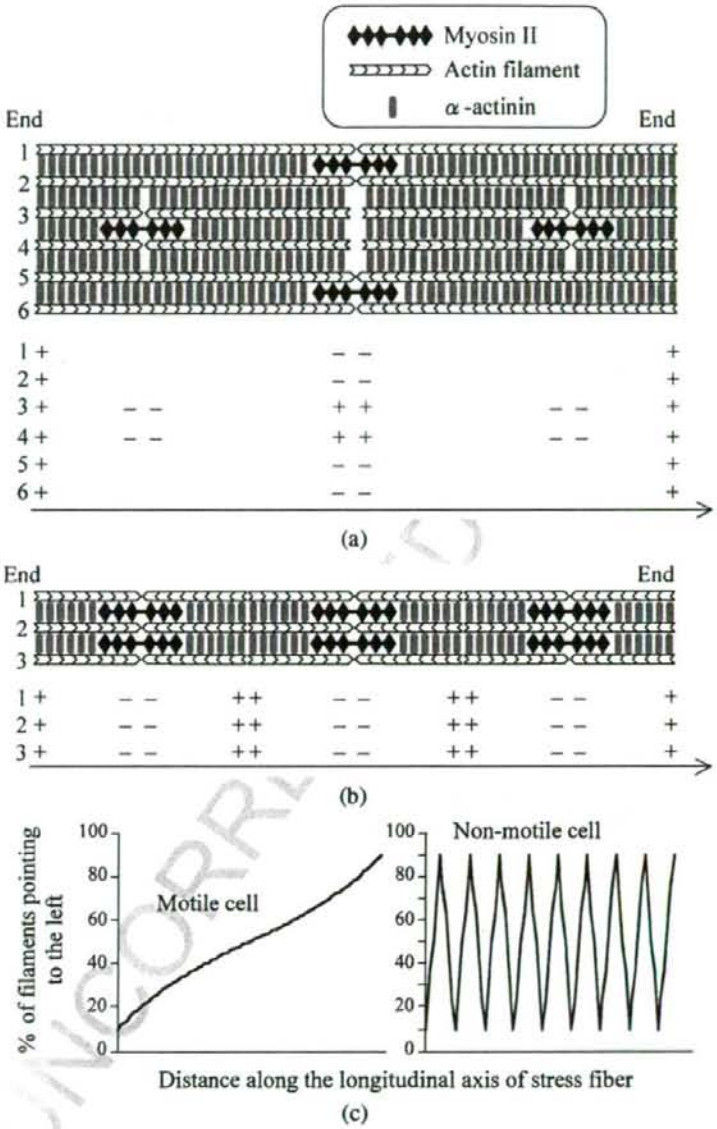

Fig. 2. Schematic drawing of the structural differences between the stress fiber in motile cells and non-motile cells based on Cramer's observations [6]. (a) Ventral stress fiber in motile cells, showing orientations of actin polarity. (b) Ventral stress fibers in non-motile cells. (c) Stress fibers in motile cells have a graded polarity pattern along the long axis (left), whereas those in non-motile cells have a periodic alternation similar to a muscle sarcomere. Modified from Cramer et al. [6] with permission of the copyright holder (The Rockefeller University Press).

observations. In the ventral region of migrating cells having inverted triangular morphology (primary fibroblasts), predominant orientations of individual actin filaments gradually alter along stress fibers. Specifically, barbed ends of actin filaments present at the ends of a stress fiber are directed toward focal adhesions (Fig. 2(a)). Around middle regions of the same stress fiber, the actin filament orientations are mixed, with the result that stress fibers in the ventral region of the motile fibroblasts exhibit a graded polarity pattern (Fig. 2(c)).

In contrast, stress fibers in the ventral region of non-motile cells (PtK2 cells) typically show a periodic alternation of the polarity (Fig. 2(b)). Reflecting this, myosin II and α-actinin appear alternately along stress fibers (Figs 2(c) and 3), similar to the organization of the muscle sarcomere (Fig. 4). The spatial periodicity is 0.9 μm in epithelial cells (PtK2 cells) and 1.5 μm in fibroblasts (Gerbil fibroma) [51]. The muscle sarcomeric configuration suggests that the stress fiber in the ventral region of non-motile cells, which is the subject of this commentary, is highly contractile and plays essential roles in isometric tension generation and resultant ECM assembly [36], whereas the ventral stress fiber in motile cells seems less suitable for generation of such static isometric tensions [48]. This review does not touch on the stress fibers present at other portions of non-motile cells, such as apical stress fibers running between the ventral and apical cell membranes, which become particularly prominent in response to fluid shear stress [26,27,30].

Stress fibers in the cytoplasm are a highly dynamic structure even in stationary cells [31,47,49], implying that such rapid association/dissociation kinetics of molecules may be essential for the formation and contractility of the stress fibers [28]. Live cell microscopy focusing on how stress fibers are assembled and disassembled may provide hints on the polarity of individual actin filaments. Hotulainen and Lappalainen [21] observed dynamics during stress fiber assembly, though it was for motile cells (U2OS cells) similar to fish keratocytes in shape having half-moon morphology [14]. They found that actin polymerization towards the cytoplasm was driven by formin (mDia1/DRF1) at focal complexes (i.e., small focal adhesions), and that connections of multiple actin bundles followed by their own contractions yield a stress fiber running between separate focal complexes in ventral regions. On the other hand, the assembly mechanism of the stress fiber in non-motile cells remains unclear; yet, another actin bundle in motile

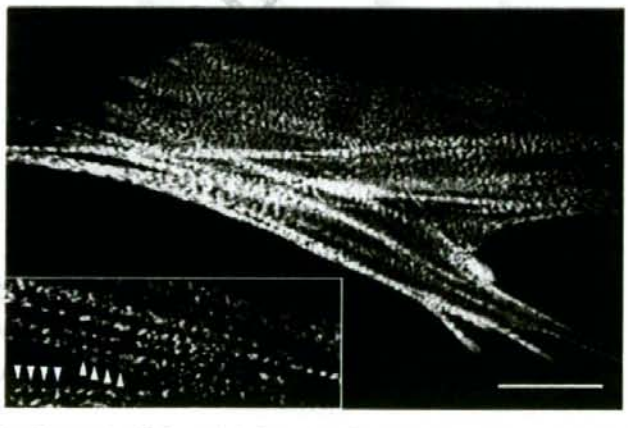

Fig. 3. A smooth muscle cell expressing GFP-α-actinin. Bar: 10 μm. Inset: magnified view; arrowheads denote periodic staining patterns seen along stress fibers.

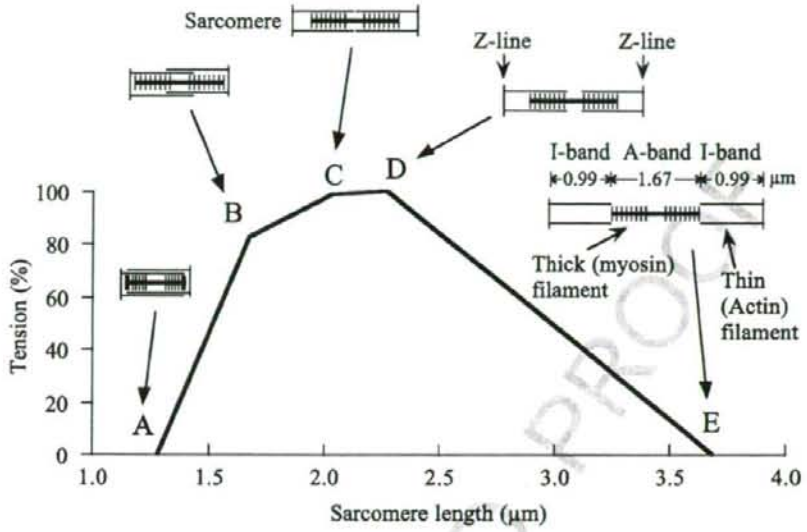

Fig. 4. Active tension generated by muscle sarcomere as a function of its length. Modified from Fung [11] with permission of the copyright holder (Springer).

cells, generated in the proximity of the cell membrane and referred to as transverse arc, has an alternate α-actinin–myosin II structure [7,21]. This transverse arc finally becomes the ventral stress fiber in motile cells having focal adhesions at both ends, thus similar in structure to the stress fiber in non-motile cells. Judging from the similar structures, the unknown assembly mechanism of the stress fiber in non-motile cells may be comparable to that of the ventral stress fiber in motile U2OS cells. In addition, Hirata et al. [20] observed the dynamics of actin bundle formation from individual actin filaments using semi-intact fibroblast cells, demonstrating that stress fibers are aligned parallel to the direction of externally applied tension.

3. Isometric tension and its relationship to assembly/disassembly

Hereafter, stress fibers in non-motile cells are the topics of discussion. Stress fibers are anchored to ECM at both ends via focal adhesions. Actomyosin contraction then produces isometric tension even in the absence of extracellular forces. Activation of myosin regulatory light chain (MLC) by Rho-kinase is responsible for the contraction, which modulates organization of stress fibers and focal adhesions [3]. Rho-kinase phosphorylates MLC directly as well as through inhibition of myosin phosphatase [24]. Meanwhile, it has been reported that calmodulin and MLC kinase (MLCK) specifically activate stress fibers lying at the cell periphery in fibroblasts in a Ca^{2+}-dependent manner [28]. They demonstrated that more rapid and extensive stress fiber contraction is induced by MLCK than by Rho-kinase. This selectivity probably holds true for endothelial cells as well because inhibition of Rho-kinase activity by Y27632 attenuated stress fiber formation particularly in central regions of the cells [31]. Different from the traction force generated by stress fibers in motile cells that is less suited for static contraction

[13,48], the isometric contraction plays critical roles in ECM assembly and resultant wound healing [16,19,64]. The MLCK-regulating contraction of peripheral stress fibers might be used for the maintenance of intercellular junctions, rather than wound healing, because those thick peripheral stress fibers or dense peripheral bands become prominent in confluent cells. Katoh et al. [28] suggested that the Ca^{2+}-regulating MLCK system is used to generate rapid contraction because Ca^{2+} release in cells is rapid and transient in general. Meanwhile, they considered that the Ca^{2+}-independent Rho-kinase system plays a major role in maintaining sustained contraction (and hence isometric contraction) in cells because, once MLC is phosphorylated, the activated state allowing contraction can be maintained by inhibiting the myosin phosphatase.

Immediate disassembly of stress fibers occurs when the tension is released by compressing. Costa et al. [6] revealed the existence of a threshold strain value required for inducing the tension-dependent disassembly. They observed, just before the occurrence of the disassembly, buckling of stress fibers in non-motile endothelial cells after compressive loading. Reasoning that the buckling occurred at their unloaded slack length, stress fibers were estimated to have a 15–26% prestrain. The variability of the value was possibly dependent on where the stress fibers were located in cells. Sato et al. [52] quantified by strain analysis on each fiber in osteoblastic cells that a compressive strain of ~20% induced disassembly. Furthermore, Lu et al. [39] found that the prestrain of stress fibers in endothelial cells increased from 10% to 26% when treated with 2 nM calyculin A that is a serine/threonine phosphatase inhibitor elevating MLC phosphorylation, and on the other hand decreased to 5% when treated with 10 μM blebbistatin that is a selective inhibitor of actomyosin interactions with a high affinity for myosin II [49]. These results indicate that stress fibers under isometric contraction have a definite tensional strain dependent on the degree of actomyosin interaction. It is, however, important to note that the matter may not be so simple since stress fibers after severed at the middle regions by laser cutting retracted due to existing tension but were not disassembled, although the tension release was transmitted to the end focal adhesions via the stress fibers [35].

Goffin et al. [16] indicated that not only strain but also tensional stress is kept an intrinsic value in myofibroblasts. They found that an ~12 nN/μm^2-tensional stress (i.e., force per unit focal adhesion area) exists at "supermature" focal adhesions [19] having large focal adhesion sizes (>7.5 μm^2), whereas a stress of only 3.8 nN/μm^2 exists at small focal adhesions or focal complexes (≤7.5 μm^2). With the changes in area size, stress fibers connecting serially the focal adhesions thus seem to keep the tensional stress as well as strain constant. The higher stress in large focal adhesions compared to small focal complexes was realized firstly by remodeling of ECM to create larger surfaces for adhesion that permit efficient tension transmission and development of stress fibers. Subsequently, the high contractility was enhanced by recruitment of α-smooth muscle actin, suitable for generating high contractility [18], to the stress fibers preformed from β-actin. The change in actin isoforms depending on mechanical conditions seems similar to the isoform changes from β-actin or γ-actin to α-actin seen during skeletal or cardiac muscle sarcomere assembly [11,38].

The phenomenon that constant prestrain and prestress are maintained, therefore, indicates that cells keep a mechanical homeostasis [23,44] associated with strain and stress in stress fibers. The jump of the maintained prestress, reported by Goffin et al. [16], from small focal complexes (3.8 nN/μm^2) to supermature focal adhesions (12 nN/μm^2) could be interpreted, from the standpoint of physics, as a transition from one equilibrium state to another: in each equilibrium state, a certain definite strain or stress should be kept. Cells may thus adapt to a slight change in the environment while keeping the mechanical homeostasis only using existing proteins. Actually, it is known that the size of mature focal adhesions reversibly increases and decreases as a function of applied force [15]. Meanwhile, if the change in the

environment were large enough to cause a transition to another equilibrium state where a new mechanical balance within the stress fiber is needed to keep the structure, the cells may adapt to the environment by modulating their molecular compositions just as is done by the recruitment of α-smooth muscle actin. Stress fibers under isometric contraction are actually accompanied by rapid molecular exchanges of α-actinin and myosin with the ones in the surrounding cytoplasm [49]. Mechanical stimuli-induced deviations from an equilibrium state (or a homeostatic state) associated with the apparently static but actually dynamic isometric conditions (such as alterations in stress) may thus cause the mechanosensitive responses of stress fibers.

Why, then, is stress or strain kept constant instead of force? Actin filaments are bundled in parallel by α-actinin and myosin to form stress fibers, and the bundling is strengthened at the periphery of stress fibers where the cross-linking (with structural proteins talin and vinculin [3,15]) is rich in quantity and quality [49,61]. Focal adhesions as a mechanosensitive element [15,25,53] might be thus affected by stress having an interaction surface (because all of the paralleled actin filaments probably deform the focal adhesions together) rather than by force unrelated to cross-sectional area. Meanwhile, stress and strain are a concept of continuum mechanics to be exact. Considering the individual molecules, stress fibers having higher-order structures are not uniform materials. Each mechanosensitive element within stress fibers, such as α-smooth muscle actin [16] might sense tensional force or elongation (or force-induced conformational change that exposes cryptic binding or phosphorylation sites) in respective actin filaments or their associated proteins rather than the stress or strain detected at the whole stress fiber scale. As for mechanosensitive elements responsible for the stress fiber disassembly, one of the potential candidates is cofilin, which colocalizes with actin and conducts severing and possibly depolymerization [46,54]. These actin-associated proteins might be regulated by tensions in each actin filament as well.

4. Biomechanical properties in the cytoplasm

Soft substrates made by microfabrication have allowed quantification of the magnitude of isometric tension in stress fibers [57]. These measurements have demonstrated that tensions of the order of $\sim$1–40 nN in magnitude, depending on the size of large focal adhesions, are exerted on the substrate in smooth muscle cells. Single actin filaments *in vitro* are able to bear $\sim$600 pN at the maximum [58]. Forces generated by single myosin heads along actin filaments are on the order of $\sim$1–10 pN [32]. However, it remains unclear how tensions are borne and transmitted within stress fibers under isometric contraction. From modeling approach, force balances in one sarcomeric unit in stress fibers have recently been discussed by considering another structural protein, titin, similar to the titin or connectin that works as an elastic element in striated muscle [4,55]. Force balances on a scale that includes interactions between stress fibers and focal adhesions were also reported, focusing on Rho-kinase-mediated spatially different contractions of actomyosin [2]. Force balance in stress fibers and its role in various macroscopic mechanical behaviors were also discussed from a tensegrity approach [41].

The lack of our knowledge about the force balance and transmission within stress fibers is partly because the mechanical properties of stress fibers were unclear. Recently, however, there have been increasing data on them. Kumar et al. [35] evaluated viscoelastic properties of stress fibers in living endothelial cells from their retraction behavior seen after being severed by laser cutting. The retraction was slowed or virtually abolished by inhibition of Rho-kinase or calmodulin/MLCK, respectively. Lu et al. [40] measured transverse (perpendicular to the longitudinal length) elastic modulus of individual stress fibers in living endothelial cells by indentation using an atomic force microscope. They revealed

that the elastic modulus of stress fibers, in which the contractile level was decreased with blebbistatin, was smaller than those in which the contractile level was increased with calyculin A. The elastic modulus was in the range of ~10 kPa, whereas the smallest values reported by Deguchi et al. [8,10] on stress fibers isolated from cells was ~300 kPa. One major difference between Lu's and Deguchi's experiments is that the former measured a transverse elastic modulus based on a small indentation depth of 200 nm while the cells were subjected to unidirectional stretch of ~8%; meanwhile, the latter measured a longitudinal elastic modulus based on ~20% axial stretch. As the stress fiber is undoubtedly an anisotropic material in which filamentous structures are bundled more or less in parallel, it seems reasonable to have elastic modulus of such different magnitudes depending on the loading direction.

Focusing on the same stress fibers inside cells, Lu's data demonstrated that the elastic modulus after the contractile level was increased was larger in the peripheral regions than that in the central regions [40]. This heterogeneous distribution of the elastic modulus along the long axis of individual stress fibers may be comparable to the non-uniform deformation of stress fibers, reported by Peterson et al. [49] after enhancement of contraction by calyculin A. They demonstrated that peripheral stress fibers shortened in length, whereas central ones were elongated probably due to passive stretching caused by stronger peripheral contraction. We touch on this topic more in detail in the following section.

5. Non-uniform contraction behavior

Why is the non-uniform deformation generated in the same stress fibers, even though they have periodic and hence regular sarcomeric structures along the long axis in non-motile cells? This still remains unclear; however, the origin has been discussed from various modeling approaches. Besser and Schwarz [2] assumed that Rho-kinase that phosphorylates MLC is rich in concentration around the cell periphery, thereby leading to higher stress fiber contraction at the periphery compared to the central region. This assumption came from ideas that the guanine nucleotide exchange factor for RhoA is activated at focal adhesions; and then activated GTP-bound Rho, the upstream signal of Rho-kinase, becomes richer in concentration near the focal adhesions rather than the central region. The spatial difference in Rho-kinase concentration is, however, still controversial as RhoA and Rho-kinase were reported to exist along the stress fibers [28]. Moreover, the myosin-binding subunit of myosin phosphatase (phosphorylated by Rho-kinase to inhibit the activity of this enzyme and to activate MLC accordingly) was also associated with stress fibers [24,42]. To account for the non-uniform deformation, other modeling studies [41,55] assumed a parameter by which the contractile force becomes stronger near the periphery than the central region. The phosphorylation level of MLC is indeed higher around the periphery than the central region [49,61], which may support this assumption.

Nevertheless, no mechanism has yet appeared that describes why MLC should be higher in concentration and be activated more at the peripheral region of stress fibers than the central region. The stress fiber assembly process (of motile cells) basically consists of mDia-based elongations and subsequent connections with different actin bundles followed by their actomyosin contraction [21,45]. Myosin movements along actin filaments would also play a role in the stress fiber assembly [59]. However, these mechanisms do not provide the reason for the non-uniform MLC concentration and activation. Interestingly, structural mechanics-based considerations (Deguchi, unpublished data) indicate that a higher stretching strain is produced in central than in peripheral regions because a certain frictional force should be present at the interface between a stress fiber and surrounding cytoplasm when there is a relative displacement to each other [9,35,47]. Such non-uniform deformations can appear even without the assumptions on

non-uniform signal concentrations or non-uniform contractile/mechanical properties depending on the positions in the stress fiber, as were postulated in previous reports [2,41,55]. Thus, tension in stress fibers may not be distributed uniformly along the axial length. This theoretical consideration could also explain the mechanism of the spatially non-uniform molecular exchange activities of myosin and α-actinin in non-motile cells where molecular exchanges are more frequent in central regions [49], because a high (but physiological) stretching strain seems to induce frequent molecular turnovers [16,63,64].

6. Biomechanical properties characterized *in vitro*

Though stress fibers are highly dynamic in the cytoplasm as mentioned earlier, Katoh et al. [29] demonstrated that stress fibers isolated from fibroblasts, by low ionic strength solution and detergent extractions, are stable and are not disassembled even without tension. The use of isolated stress fibers thus helps understand the component composition and characterization of the mechanical properties excluding effects of the surrounding cytoplasm and turnovers. The isolated stress fiber showed contractile behavior whose magnitude was dependent on the concentration of Mg^{2+}-ATP. Detergent extraction using Triton X-100 readily dissolved both RhoA and Rho-kinase; hence, as mentioned earlier, such stress fibers showed only Ca^{2+}-dependent contractions. Meanwhile, fibers subjected to detergent extraction using glycerol were capable of contracting both in the presence and absence of Ca^{2+} since the Rho-kinase-mediated contraction, independent of Ca^{2+}, remained unchanged.

Surprisingly, the isolated stress fiber shortened to 20% of the original length, without molecular turnover or exchanges with cytoplasmic constituents [28,29]. Sarcomeres in striated muscles cannot shorten to that extent because of the existence of A-bands consisting mostly of myosin thick filaments (Fig. 4). Stress fibers in non-motile cells have a sarcomeric structure (Figs 2 and 3); yet, they may be less organized compared to the muscle sarcomere [12]. As for the difference between the stress fibers in non-motile cells and in muscle sarcomere, Peterson et al. [49] have proposed that α-actinin in stress fibers is not confined to a relatively narrow Z-line structure, but extends into an equivalent of the muscle I-band while binding to actin regions that do not overlap with myosin (Fig. 2).

In addition to the tension caused by isometric contraction, stress fibers in vascular endothelial and smooth muscle cells are subjected to cyclic stretching *in vivo* due to pulsatile blood pressure. Tensile properties of stress fibers are thus important to assess the resistance to the stretching and the ability of tension transmission that may directly activate remote mechanosensitive sites [17,22,43,60]. Using a pair of cantilevers as a micromanipulation tool, Deguchi et al. [8–10] evaluated a longitudinal elastic modulus of single stress fibers isolated from endothelial cells ($\sim$300 kPa) and smooth muscle cells ($\sim$1.45 MPa) assuming that stress fibers are a uniform structure having a certain cross-sectional area ($\sim$0.05 μm^2) estimated based on electron microscopy (Fig. 5). These values, even in the absence of Mg^{2+}-ATP that unties myosin from actin filaments, are much smaller in magnitude compared to single actin filaments having a longitudinal elastic modulus of $\sim$1 GPa [33]. Tensional loadings of $\sim$10-nN order of magnitude were required for stretching single stress fibers, whereas $\sim$100-pN tensions were enough for individual actin filaments to obtain their force–strain curves [37]. Since the slope of the force–strain curve (corresponding to elastic modulus) in Deguchi's data increases as stretch proceeds, stress fibers may have a loose structure in which dominant stress-bearing components vary with strain. Lu et al. [40] also reported a transverse elastic modulus of stress fibers in living cells that nonlinearly increased depending on the magnitude of substrate stretch.

The single proteins (i.e., actin filaments) and composite structures (i.e., stress fibers) thus differ in elastic modulus and force transmission ability. Cramer et al. [7] found that stress fibers in motile cells

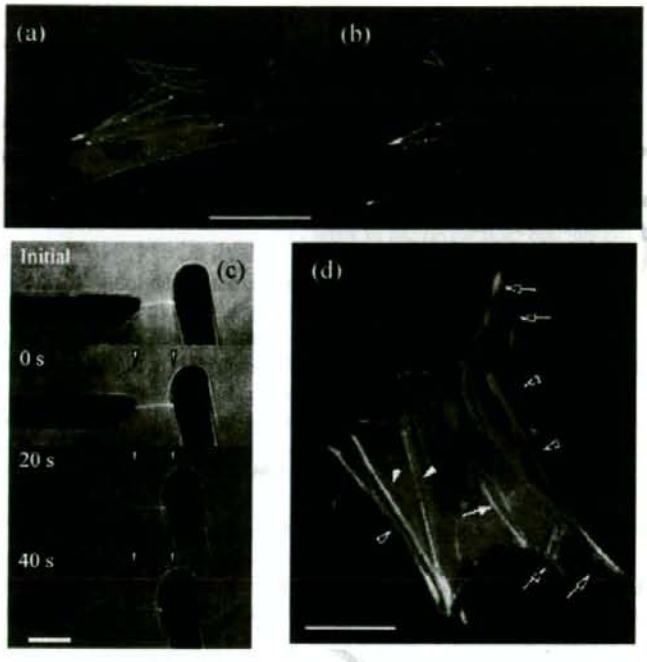

Fig. 5. Measurements on isolated stress fibers. (a) A smooth muscle cells expressing GFP-actin and RFP-focal adhesion kinase. (b) The same cell after cytoplasmic constituents are removed by chemical treatments except for the remaining stress fibers and focal adhesions. (c) Tensile test of a single stress fiber. Arrows indicate the initial positions of the cantilevers used for micromanipulation. (d) Superimposed images of smooth muscle cells before (green) and after (red) the cytoplasm except for ventral stress fibers and focal adhesions that were removed by chemical treatments. Some stress fibers (open arrowheads) were removed after the treatment, and thick stress fibers (closed arrowheads) pivoted outward. The positions of focal adhesions located at the terminal of stress fibers remained unchanged as shown by the yellow color. This result indicates that before the removal of the cytoplasm stress fibers had tensional prestress, and that they deform to reduce strain energy after some constraints are removed. Scale bars: 20 μm. Reproduced with permission of the copyright holder (Tech Science Press). (The colors are visible in the online version of the article.)

contain ~10–30 actin filaments. However, as far as the authors know, quantification of the number of associated filaments inside stress fibers of non-motile cells has not yet been achieved, although the amounts of respective molecular compositions within stress fibers were investigated [29]. As detailed mechanical structure (including boundary conditions between structural molecules) and force transmission inside stress fibers are largely unknown [1], qualitative and quantitative understating of such mechanical hierarchies will be a subject of future investigations.

7. Concluding remarks

In this review, starting from the clarification of which actin bundles are the subject of interest here, we discussed the biomechanical properties of stress fibers of non-motile cells, including isometric contraction, prestrain/prestress, elastic properties, and the relationships between those properties and the

dynamic exchanges of associated molecules occurring frequently in the cytoplasm. By keeping an intracellular mechanical homeostasis through the maintenance of the isometric contraction or remodeling of focal adhesions and stress fibers, cells seem to adapt to the surrounding mechanical environment.

Acknowledgements

The authors thank Kazushi Ito and Tsubasa Matsui for discussions. The authors apologize to workers in this field for having omitted many important papers owing to space constraints.

References

[1] M. Bathe, C. Heussinger, M.M.A.E. Claessens, A.R. Bausch et al., Cytoskeletal bundle mechanics, *Biophys. J.* **94** (2008), 2955–2964.
[2] A. Besser and U. Schwarz, Coupling biochemistry and mechanics in cell adhesion: a model for inhomogeneous stress fiber contraction, *New J. Phys.* **9** (2007), 1–27.
[3] K. Burridge, M. Chrzanowska-Wodnicka and C. Zhong, Focal adhesion assembly, *Trends Cell. Biol.* **7** (1997), 342–347.
[4] P.J. Cavnar, S.G. Olenych and T.C. Keller, Molecular identification and localization of cellular titin, a novel titin isoform in the fibroblast stress fiber, *Cell Motil. Cytoskel.* **64** (2007), 418–433.
[5] P. Chardin, P. Boquet, P. Madaule, M.R. Popoff et al., The mammalian G protein rhoC is ADP-ribosylated by clostridium botulinum exoenzyme C3 and affects actin microfilaments in vero cells, *EMBO J.* **8** (1989), 1087–1092.
[6] K.D. Costa, W.J. Hucker and F.C. Yin, Buckling of actin stress fibers: a new wrinkle in the cytoskeletal tapestry, *Cell Motil. Cytoskel.* **52** (2002), 266–274.
[7] L.P. Cramer, M. Siebert and T.J. Mitchison, Identification of novel graded polarity actin filament bundles in locomoting heart fibroblasts: implications for the generation of motile force, *J. Cell Biol.* **136** (1997), 1287–1305.
[8] S. Deguchi, T. Ohashi and M. Sato, Evaluation of tension in actin bundle of endothelial cells based on preexisting strain and tensile properties measurements, *Mol. Cell. Biomech.* **2** (2005), 125–133.
[9] S. Deguchi, T. Ohashi and M. Sato, Intracellular stress transmission through actin stress fiber network in adherent vascular cells, *Mol. Cell. Biomech.* **2** (2005), 205–216.
[10] S. Deguchi, T. Ohashi and M. Sato, Tensile properties of single stress fibers isolated from cultured vascular smooth muscle cells, *J. Biomech.* **39** (2006), 2603–2610.
[11] A.A. Dlugosz, P.B. Antin, V.T. Nachimas and H. Holtzer, The relationship between stress-fibre-like structures and nascent myofibrils in cultured cardiac myocytes, *J. Cell Biol.* **99** (1984), 2268–2278.
[12] Y.C. Fung, *Biomechanics Motion, Flow, Stress, and Growth*, Springer-Verlag, 1990, pp. 158–159.
[13] C.G. Galbraith and M.P. Sheetz, Forces on adhesive contacts affect cell function, *Curr. Opin. Cell Biol.* **10** (1998), 566–571.
[14] C.G. Galbraith and M.P. Sheetz, Keratocytes pull with similar forces on their dorsal and ventral surfaces, *J. Cell Biol.* **147** (1999), 1313–1324.
[15] B. Geiger and A. Bershadsky, Assembly and mechanosensory function of focal contacts, *Curr. Opin. Cell Biol.* **13** (2001), 584–592.
[16] J.M. Goffin, P. Pittet, G. Csucs, J.W. Lussi et al., Focal adhesion size controls tension-dependent recruitment of alpha-smooth muscle actin to stress fibers, *J. Cell Biol.* **172** (2006), 259–268.
[17] K. Hayakawa, H. Tatsumi and M. Sokabe, Actin stress fibers transmit and focus force to activate mechanosensitive channels, *J. Cell Sci.* **121** (2008), 496–503.
[18] B. Hinz, G. Celetta, J.J. Tomasek, G. Gabbiani and C. Chaponnier, Alpha-smooth muscle actin expressions upregulates fibroblast contractile activity, *Mol. Biol. Cell* **12** (2001), 2730–2741.
[19] B. Hinz and G. Gabbiani, Mechanisms of force generation and transmission by myofibroblasts, *Curr. Opin. Biotechnol.* **14** (2003), 538–546.
[20] H. Hirata, H. Tatsumi and M. Sokabe, Dynamics of actin filaments during tension-dependent formation of actin bundles, *Biochim. Biophys. Acta* **1770** (2007), 1115–1127.
[21] P. Hotulainen and P. Lappalainen, Stress fibers are generated by two distinct actin assembly mechanisms in motile cells, *J. Cell Biol.* **173** (2006), 383–394.
[22] S. Hu, J. Chen, B. Fabry, Y. Numaguchi et al., Intracellular tomography reveals stress focusing and structural anisotropy in cytoskeleton of living cells, *Am. J. Physiol. Cell Physiol.* **285** (2003), C1082–C1090.

[23] J.D. Humphrey, Vascular adaptation and mechanical homeostasis at tissue, cellular, and sub-cellular levels, *Cell Biochem. Biophys.* **50** (2008), 53–78.
[24] N. Inagaki, M. Nishizawa, M. Ito, M. Fujioka et al., Myosin binding subunit of smooth muscle myosin phosphatase at the cell–cell adhesion sites in MDCK cells, *Biochem. Biophys. Res. Commun.* **230** (1997), 552–556.
[25] D.E. Ingber, Tensegrity II. How structural networks influence cellular information processing networks, *J. Cell Sci.* **116** (2003), 1397–1408.
[26] Y. Kano, K. Katoh and K. Fujiwara, Lateral zone of cell–cell adhesion as the major fluid shear stress-related signal transduction site, *Circ. Res.* **86** (2000), 425–433.
[27] Y. Kano, K. Katoh, M. Masuda and K. Fujiwara, Macromolecular composition of stress fiber-plasma membrane attachment sites in endothelial cells *in situ*, *Circ. Res.* **79** (1996), 1000–1006.
[28] K. Katoh, Y. Kano, M. Amano, H. Onishi et al., Rho-kinase-mediated contraction of isolated stress fibers, *J. Cell Biol.* **153** (2001), 569–583.
[29] K. Katoh, Y. Kano, M. Masuda, H. Onishi and K. Fujiwara, Isolation and contraction of the stress fiber, *Mol. Biol. Cell* **9** (1998), 1919–1938.
[30] K. Katoh, M. Masuda, Y. Kano, Y. Jinguji and K. Fujiwara, Focal adhesion proteins associated with apical stress fibers of human fibroblasts, *Cell Motil. Cytoskel.* **31** (1995), 177–195.
[31] R. Kaunas, P. Nguyen, S. Usami and S. Chien, Cooperative effects of Rho and mechanical stretch on stress fiber organization, *Proc. Natl. Acad. Sci. USA* **102** (2005), 15895–15900.
[32] A. Kishino and T. Yanagida, Force measurements by micromanipulation of a single actin filament by glass needles, *Nature* **334** (1988), 74–76.
[33] H. Kojima, A. Ishijima and T. Yanagida, Direct measurement of stiffness of single actin filaments with and without tropomyosin by *in vitro* nanomanipulation, *Proc. Natl. Acad. Sci. USA* **91** (1994), 12962–12966.
[34] Y.E. Kreis and W. Birchmeier, Stress fiber sarcomeres of fibroblasts are contractile, *Cell* **22** (1980), 555–561.
[35] S. Kumar, I.Z. Maxwell, A. Heisterkamp, T.R. Polte et al., Viscoelastic retraction of single living stress fibers and its impact on cell shape, cytoskeletal organization, and extracellular matrix mechanics, *Biophys. J.* **90** (2006), 3762–3773.
[36] E. Lazarides and K. Burridge, α-Actinin: immunofluorescent localization of a muscle structural protein in nonmuscle cells, *Cell* **6** (1975), 289–298.
[37] X. Liu and G.H. Pollack, Mechanics of F-actin characterized with microfabricated cantilevers, *Biophys. J.* **83** (2002), 2705–2715.
[38] C.M. Lloyd, M.M. Berendse, D.G. Lloyd, G. Schevzov and M.D. Grounds, A novel role for non-muscle γ-actin in skeletal muscle sarcomere assembly, *Exp. Cell Res.* **297** (2002), 82–96.
[39] L. Lu, Y. Feng, W.J. Hucker, S.J. Oswald, G.D. Longmore and F.C. Yin, Actin stress fiber pre-extension in human aortic endothelial cells, *Cell. Motil. Cytoskel.* **65** (2008), 281–294.
[40] L. Lu, S.J. Oswald, H. Ngu and F.C. Yin, Mechanical properties of actin stress fibers in living cells, *Biophys. J.* **95** (2008), 6060–6071.
[41] Y. Luo, X. Xua, T. Lele, S. Kumar and D.E. Ingber, A multi-modular tensegrity model of an actin stress fiber, *J. Biomech.* **41** (2008), 2379–2387.
[42] K. Murata, K. Hirano, E. Villa-Moruzzi, D.J. Hartshorne and D.L. Brautigan, Differential localization of myosin and myosin phosphatase subunits in smooth muscle cells and migrating fibroblasts, *Mol. Biol. Cell* **8** (1997), 663–673.
[43] S. Na, O. Collin, F. Chowdhury, B. Tay et al., Rapid signal transduction in living cells is a unique feature of mechanotransduction, *Proc. Natl. Acad. Sci. USA* **105** (2008), 6626–6631.
[44] S. Na, G.A. Meininger and J.D. Humphrey, Theoretical model for F-actin remodeling in vascular smooth muscle cells subjected to cyclic stretch, *J. Theor. Biol.* **246** (2007), 87–99.
[45] P. Naumanen, P. Lappalainen and P. Hotulainen, Mechanisms of actin stress fibre assembly, *J. Microsc.* **231** (2008), 446–454.
[46] K. Ohashi, K. Nagata, M. Maekawa, T. Ishizaki et al., Rho-associated kinase ROCK activates LIM-kinase 1 by phosphorylation at threonine 508 within the activation loop, *J. Biol. Chem.* **275** (2000), 3577–3582.
[47] E.A. Osborn, A. Rabodzey, C.F. Dewey Jr. and J.H. Hartwig, Endothelial actin cytoskeleton remodeling during mechanostimulation with fluid shear stress, *Am. J. Physiol. Cell Physiol.* **290** (2006), C444–C452.
[48] S. Pellegrin and H. Mellor, Actin stress fibres, *J. Cell Sci.* **120** (2007), 3491–3499.
[49] L.J. Peterson, Z. Rajfur, A.S. Maddox, C.D. Freel et al., Simultaneous stretching and contraction of stress fibers *in vivo*, *Mol. Biol. Cell* **15** (2004), 3497–3508.
[50] A.J. Ridley and A. Hall, The small GTP-binding protein rho regulates the assembly of focal adhesions and actin stress fibers in response to growth factors, *Cell* **70** (1992), 389–399.
[51] J.W. Sanger, J.M. Sanger and B.M. Jockusch, Differences in the stress fibers fibroblasts and epithelial cells, *J. Cell Biol.* **96** (1983), 961–969.
[52] K. Sato, T. Adachi, M. Matsuo and Y. Tomita, Quantitative evaluation of threshold fiber strain that induces reorganization of cytoskeletal actin fiber structure in osteoblastic cells, *J. Biomech.* **38** (2005), 1895–1901.

[53] T. Shemesh, B. Geiger, A.D. Bershadsky and M.M. Kozlov, Focal adhesions as mechanosensors: a physical mechanism, *Proc. Natl. Acad. Sci. USA* **102** (2005), 12383–12388.
[54] M. Sokabe, K. Hayakawa and H. Tatsumi, Differentiation of two types of mechanosensors in endothelial cells, *J. Biomech.* **39** (2006), S311.
[55] M.R. Stachowiak and B. O'Shaughnessy, Kinetics of stress fibers, *New J. Phys.* **10** (2008), 025002.
[56] A.F. Straight, A. Cheung, J. Limouze, I. Chen et al., Dissecting temporal and spatial control of cytokinesis with a myosin II inhibitor, *Science* **299** (2003), 1743–1747.
[57] J.L. Tan, J. Tien, D.M. Pirone, D.S. Gray et al., Cells lying on a bed of microneedles: an approach to isolate mechanical force, *Proc. Natl. Acad. Sci. USA* **100** (2003), 1484–1489.
[58] Y. Tsuda, H. Yasutake, A. Ishijima and T. Yanagida, Torsional rigidity of single actin filaments and actin–actin bond breaking force under torsion measured directly by *in vitro* micromanipulation, *Proc. Natl. Acad. Sci. USA* **93** (1996), 12937–12942.
[59] A.B. Verkhovsky, T.M. Svitkina and G.G. Borisy, Polarity sorting of actin filaments in cytochalasin-treated fibroblasts, *J. Cell Sci.* **110** (1997), 1693–1704.
[60] N. Wang and Z. Suo, Long-distance propagation of forces in a cell, *Biochem. Biophys. Res. Commun.* **328** (2005), 1133–1138.
[61] T. Watanabe, H. Hosoya and S. Yonemura, Regulation of myosin II dynamics by phosphorylation and dephosphorylation of its light chain in epithelial cells, *Mol. Biol. Cell* **18** (2007), 605–616.
[62] B. Wojciak-Stothard and A.J. Ridley, Shear stress-induced endothelial cell polarization is mediated by Rho and Rac but not Cdc42 or PI 3-kinases, *J. Cell Biol.* **161** (2003), 429–439.
[63] M. Yoshigi, L.M. Hoffman, C.C. Jensen, H.J. Yost and M.C. Beckerle, Mechanical force mobilizes zyxin from focal adhesions to actin filaments and regulates cytoskeletal reinforcement, *J. Cell Biol.* **171** (2005), 209–215.
[64] C. Zhong, M. Chrzanowska-Wodnicka, J. Brown, A. Shaub et al., Rho-mediated contractility exposes a cryptic site in fibronectin and induces fibronectin matrix assembly, *J. Cell Biol.* **141** (1998), 539–551.

J Gastroenterol 2008; 43:538–549
DOI 10.1007/s00535-008-2188-3

Journal of Gastroenterology

Peroxisome proliferator-activated receptor α activates cyclooxygenase-2 gene transcription through bile acid transport in human colorectal cancer cell lines

Hiroshi Oshio[1], Takaaki Abe[2,3], Tohru Onogawa[1], Hideo Ohtsuka[1], Takeaki Sato[1], Takayuki Ii[1], Kouji Fukase[1], Mitsuhisa Muto[1], Yu Katayose[1], Masaya Oikawa[1], Toshiki Rikiyama[1], Shinichi Egawa[1], and Michiaki Unno[1]

[1]Division of Gastroenterological Surgery, Department of Surgery, Tohoku University Graduate School of Medical Science, 1-1 Seiryo-machi, Aoba, Sendai 980-8574, Japan
[2]Division of Nephrology, Endocrinology, and Vascular Medicine, Department of Medicine, Tohoku University Graduate School of Medical Science, Sendai, Japan
[3]PRESTO, Japan Science and Technology Corporation (JST), Tokyo, Japan

Background. Evidence is accumulating that bile acids are involved in colon cancer development, but their molecular mechanisms remain unexplored. Bile acid has been reported to be associated with induction of the cyclooxygenase-2 (*COX-2*) gene. Because the human liver-specific organic anion transporter-2 (LST-2/OATP8/OATP1B3) is expressed in gastrointestinal cancers and might transport bile acids to the intracellular space, we studied the molecular mechanisms by which bile acids induce the transcription of *COX-2*, and the role of LST-2 in colonic cell lines. ***Methods.*** Transcriptional activity of *COX-2* was measured using a human *COX-2* promoter–luciferase assay under various concentrations of bile acids. Electrophoresis mobility shift assays (EMSAs) for peroxisome proliferator-activated receptor (PPAR) α and cyclic AMP responsive element (CRE) were performed. ***Results.*** The *COX-2* promoter was induced by lithocholic acid (LCA), deoxycholic acid (DCA), and chenodeoxycholic acid (CDCA). Deletion and site-directed mutation analyses showed that CRE is the responsive element for LCA. An adenovirus expression system revealed that LST-2 is responsible for induction of *COX-2*. By EMSA using oligonucleotides of CRE, we observed formation of a specific protein–DNA complex, which was inhibited by a specific antibody against PPARα and CRE. A PPARα-specific agonist induced transcription of *COX-2*. ***Conclusion.*** These results indicate that *COX-2* is transcriptionally activated by the addition of LCA, CDCA, and DCA and that LST-2 plays an important role by transporting bile acid to the intracellular space. Moreover, LCA-dependent *COX-2* gene activation consists of a transcriptional complex including PPARα and CRE-binding protein. Thus, this induction of *COX-2* may participate in carcinogenesis and progression of colorectal cancer cells.

Received: July 5, 2007 / Accepted: March 11, 2008
Reprint requests to: M. Unno

Key words: LST-2, OATP1B3, COX-2, PPARα, bile acid

Introduction

In 2001, we isolated human liver-specific organic anion transporter-2 (LST-2/OATP8/OATP1B3).[1] The amino acid sequence of LST-2/OATP1B3 has 79.7% sequence homology to liver specific transporter-1 (LST-1/OATP-C/OATP2/OATP1B1).[2] LST-2/OATP8/OATP1B3 also has a moderate sequence homology to both the organic anion transporter polypeptide (oatp) family and the prostaglandin (PG) transporter family. Both LST-1/OATP1B1 and LST-2/OATP8/OATP1B3 are expressed in the basolateral membrane of hepatocytes but not in other normal tissues. We revealed that these transporters play a key role in the uptake of a wide variety of endogenous and exogenous anionic compounds, including bile acids, prostaglandins, conjugated steroids, and some kinds of drugs into hepatocytes. On the other hand, we found that only LST-2/OATP8/OATP1B3, but not LST-1/OATP1B1, is expressed in a number of gastrointestinal cancers.[1] However, the role of LST-2/OATP8/OATP1B3 (hereafter, LST-2) expressed in gastrointestinal cancer cells is still unknown.

Recently, aspirin and other nonsteroidal anti-inflammatory drugs have been shown to reduce the relative risk of developing colorectal or other cancers.[3–5] The products of cyclooxygenase (COX) activity are known to be significant contributors to carcinogenesis.[6–8] COX catalyzes the synthesis of prostaglandins (PGs) from arachidonic acid. There are three different isoforms of COX. COX-1 is constitutively expressed in most tissues and appears to be responsible for various physiologic functions.[9] By contrast, COX-2 is largely absent in most normal tissues but is induced upon stimulation by inflammatory agents such as cytokines,

and also by oncogenes, growth factors, carcinogens, and tumor promoters.[10–15] Indeed, several studies have reported an association with colorectal carcinogenesis.[16,17] Several different mechanisms are potentially involved in carcinogenesis. For example, overexpression of *COX-2* contributes to colorectal carcinogenesis by promoting the invasiveness of malignant cells, inhibiting apoptosis, and supporting angiogenesis.[18–20] Furthermore, human colorectal carcinoma patients with COX-2-positive tumors show a significantly poorer prognosis than those with tumors negative for COX-2.[21] COX-3 has also been recently identified, but its function is not well characterized.[22]

It was recently demonstrated that bile acids, particularly secondary bile acids, can stimulate cell proliferation[23] and act as tumor promoters in colon carcinogenesis.[24,25] Furthermore, previous reports have suggested that endogenous bile acids are ligands for nuclear receptors, such as farnesoid X receptor (FXR), pregnane X receptor (PXR), and vitamin D receptor (VDR).[26–29] It is well known that bile acids act as signaling molecules that regulate their own biosynthesis. Peroxisome proliferator-activated receptor (PPAR) α is a member of a nuclear receptor superfamily. PPARα is activated by binding ligands, enabling it to activate gene expression by binding to PPAR response elements as heterodimers with the retinoid X receptors.[30,31] Fatty acid derivatives are natural ligands for PPARs,[32] which control lipid and glucose metabolism and have anti-inflammatory activities.[33–35] A recent study reported that bile acids also induce the expression of the *PPARα* gene via activation of FXR, an example of cross talk between the FXR and PPARα pathways.[36]

In 1998, Zhang et al.[37] reported that the dihydroxy bile acids chenodeoxycholate (CDCA) and deoxycholate (DCA) activate the transcription of *COX-2* and that this activation is associated with activator protein 1 (AP-1) and protein kinase C signaling pathway in human esophageal adenocarcinoma cells. However, it remains unclear whether LST-2 is involved in the activation of *COX-2* or how bile acids activate *COX-2*.

The purpose of the present study was to clarify the molecular mechanism by which bile acids induce the transcription of *COX-2* and the role of LST-2 in colorectal cell lines HCT116 and HT29. This induction of *COX-2* caused by bile acids may participate in carcinogenesis and the progression of colorectal cancer cells.

Methods

Materials

All bile acids were purchased from Sigma (St Louis, MO, USA). They were prepared as stock solutions (0.1 mol/l) in water, except for the lithocholic acid (LCA) solution (0.1 mol/l), which was prepared in 100% ethanol. McCOY5A medium was purchased from ICN Biomedicals, (Aurora, OH, USA). The selective PPARα agonist WY14643 ([[4-chloro-6-[(2.3-dimethylphenyl)amino]-2-pyrimidinyl]thio]-acetic acid) was purchased from Cayman Chemical (Ann Arbor, MI, USA). The selective PPARβ/δ agonist GW501516 (2-methyl-4-((4-methyl-2-(4-trifluoromethylphenyl)-1,3-thiazol-5-yl)-methylsulfanyl) phenoxy-acetic acid), the selective PPARγ agonist ciglitazone ((+/–)5-[4-(1-methylcyclohexylmethoxy)benzyl] thiazolidine-2, 4-dione), and the epidermal growth factor receptor kinase inhibitor PD168393 were purchased from Calbiochem (La Jolla, CA, USA). Recombinant human epidermal growth factor was purchased from Peprotech EC (London, UK). Monoclonal antibodies of PPARα (2ZH0723), PPARγ (2ZK8713), and PPARδ (2ZK9436H) were purchased from Perseus Proteomics (Tokyo, Japan). Polyclonal antibodies against FXR (sc-13063x), PXR (sc-7739x), VDR (sc-1008), AP-1 (sc-2501), and c-Fos (sc-52x), and monoclonal antibody against cyclic AMP response element binding protein (CREB)-1 (sc-240x) were purchased from Santa Cruz Biotechnology (Santa Cruz, CA, USA).

Cells and culture

HCT116 cells were purchased from American Type Culture Collection (Rockville, MD, USA), and HT29 and HepG2 cell lines were provided by the Cell Resource Center for Biomedical Research, Tohoku University, Sendai, Japan. HCT116 cells are epithelial-like and derived from a human colon carcinoma.[38] HT29 cells are derived from a human colonic adenocarcinoma,[39] and HepG2 cells are derived from a human hepatoblastoma.[40] HCT116 cells were maintained in McCOY5A medium with 10% fetal bovine serum (FBS); HepG2 cells were maintained in Dulbecco's modified Eagle's medium (DMEM) (Sigma) with 10% FBS in a humidified atmosphere of 95% air and 5% CO2 at 37°C. The cell culture was passaged every 3 or 4 days. These cells were used between passages 3 and 25 in all experiments. It should be noted that neither LST-1/OATP1B1 nor LST-2 are expressed in HepG2 cells, while LST-2 is expressed in HCT116 and HT29.

Plasmid construction

pGL3-basic, a promoterless luciferase reporter vector was purchased from Promega (Madison, WI, USA). Several fragments of the *COX-2* promoter (–1555/+178, –1555/+178, –894/+178, –423/+178, –240/+178, –139/+178, –44/+178) were amplified by polymerase chain reaction (PCR) using human genomic DNA (Clontech Labora-

Table 1. Oligonucleotides used in the electrophoresis mobility shift assay

	NF-κB	C/EBP	CRE
Consensus	5′ NGGGGAMTTTCCNN 3′	5′RNRTKNNGMAAKNN 3′	5′NNNNSTGACGTAANN 3′
Wild type	5′TGGGGACTACCCCC 3′	5′GGCTTACGCAATTT 3′	5′AGTCATTTCGTCACA 3′
Mutant	5′TGGGCCCTACCCCC 3′	5′GGCTTACGCCGTTT 3′	5′ACAGATTTCAGTACA 3′

NF-kB, nuclear factor κB; CRE, cyclic AMP response element
under line, mutated nucleotides

tories, Palo Alto, CA, USA) as a template, with LA *Taq* DNA polymerase (TAKARA BIO, Siga, Japan). The upstream primers contained an internal *Bam*HI restriction site, and the downstream primers contained an internal *Hin*dIII restriction site. This DNA fragment was ligated into the *Bam*HI and *Hin*dIII sites of the pGL3-basic multicloning site with a sense orientation, upstream of the firefly luciferase reporter gene. Constructions of reporter plasmid for the human *COX-2* gene, COX-2-1555/Luc, COX-2-894/Luc, COX-2-423/Luc, COX-2-240/Luc, COX-2-139/Luc, and COX-2-44/Luc were prepared. The sequence identities of all constructs were verified by a CEQ2000XL DNA analysis system (Beckman Coulter, Fullerton, CA, USA). Several mutant constructs were prepared using a QuickChange Site-Direct Mutagenesis Kit (Stratagene, La Jolla, CA, USA). Mut-NFκB represents the −1555/+178 COX-2 plasmid with a mutation in the nuclear factor κB (NF-κB) site, Mut-C/EBP represents the −1555/+178 COX-2 plasmid with a mutation in the C/EBP site, and Mut-CRE represents the −1555/+178 COX-2 plasmid with a mutation in the cyclic AMP response element (CRE) site. A double mutant construct, Mut-C/EBP: CRE represents the −1555/+178 COX-2 plasmid with a mutation in the C/EBP:CRE site. The sequences of Mut-NFκB, Mut-C/EBP, Mut-CRE, Mut-C/EBP, and CRE are shown in Table 1. Plasmid DNA was isolated and purified using an EndoFree Plasmid Midi Kit (Qiagen, Hilden, Germany) according to the manufacturer's instructions. The oligonucleotide primers were synthesized at Nihon Gene Research Laboratories (Sendai, Japan).

Transfection and luciferase assay

HCT116 cells were grown to 90% confluence in 6-well plates in a cell culture dish. After removal of the medium, fresh medium, 3 μg of plasmid DNA [a human *COX-2* promoter–luciferase construct (−1555/+178)], and 6 μl of Lipofectamine 2000 (Invitrogen, Carlsbad, CA, USA) were added to the culture dish. To normalize for transfection efficiency, 20 ng of pRL-TK plasmid (Promega) coding for *Renilla* luciferase under the control of a thymidine kinase promoter was cotransfected. After 12 h, the transfection mixture was removed, and the cells were trypsinized. Full growth medium (McCOY5A with 10% FBS) was then added to the cells to inhibit the trypsin, and the cells were pelleted by centrifugation at 300 *g*. Cells were seeded into a 24-well plate, and various test agents (bile acids) were added to each well. After 24 h, the medium was removed, and then cells were washed with phosphate-buffered saline (PBS) (80 mmol/l Na_2HPO_4, 20 mmol/l NaH_2PO_4, and 100 mmol/l NaCl, pH 7.5). Passive lysis buffer (Promega) was added to each well, and the cells were lysed for 30 min. Luciferase activities were assayed using the dual luciferase reporter system (Promega) and were quantified in a Lumat LB 9507-2 luminometer (Berthold, Bad Wildbad, Germany).

Adenovirus-mediated expression of LST-2 in culture cells

In our previous work, we established adenovirus-mediated overexpression of LST-2 (submitted). This system revealed that LST-2 plays a key role in the uptake of LCA into cells (unpublished data). HepG2 cells were cultured in 24-well multiplates in 500 μl of DMEM supplemented with 10% FBS, and the cell number was adjusted to about 40×10^4 per well when these cells were infected with *AdLST-2* (*LST-2/OATP8/OATP1B3* recombinant adenovirus, termed *AdLST-2*). Infection was performed with 30 plaque forming units (pfu) of *AdLST-2*. After infection, the cell lines were incubated for 24 h in the appropriate medium for each cell line at 37°C with 5% CO2. The *COX-2* promoter–luciferase construct (−1555/+178) and pRL-TK plasmid were cotransfected, and then the luciferase activity was measured as described above. The *Adb-gal* (*b-gal* recombinant adenovirus, termed *Adb-gal*)-infected cells were used as a control.

Electrophoretic mobility shift assay

Nuclear extracts of HCT116 and HepG2 cells under the various conditions were harvested as described before.[41] For binding studies, a double-stranded oligonucleotide probe containing the CRE or C/EBP site of the *COX-2* promoter was used. The following oligonucleotides containing the CRE site of the *COX-2* promoter were synthesized: 5′-AAACAGTCATTTCGTCACATGG GCTTG-3′ (sense) and 5′-CAAGCCCATGTGACGA

AATGACTGTTT-3′ (antisense). The oligonucleotides containing the C/EBP site of the *COX-2* promoter were synthesized: 5′-CCCACCGGGCTTACGCAATTTTT TTAAGGG-3′ (sense) and 5′-CCCTTAAAAAAATT GCGTAAGCCCGGTGGG-3′ (antisense). Double-stranded oligonucleotide probes were obtained by hybridizing single-stranded complementary oligonucleotides. The annealed oligonucleotide was phosphorylated at the 5′-end with [g-^{32}P]ATP and T4 polynucleotide kinase. The binding reaction was performed by incubating 20 µg of nuclear protein in binding buffer [10 mM HEPES, pH 7.6, 0.5 mM dithiothreitol, 2.5 mM MgCl2, 0.05% (vol/vol) Nonident P-40, 10% (vol/vol) glycerol, and 50 ng/µl poly (dI-dC)] in a final volume of 10 µl for 10 min at room temperature. Then, 1.75 fmol of ^{32}P-labeled probe was added and the binding reaction was incubated at room temperature for 20 min. For competition assays, a 10- to 100-fold excess amount of unlabeled dimerized oligonucleotides was added. For supershift experiments, 2 µg of monoclonal antibodies against PPARα, PPARγ, PPARδ, and CREB-1, or polyclonal antibodies against PPARβ, FXR, PXR, VDR, AP-1, and c-Fos were added to the reaction mix. Reactions were analyzed by electrophoresis through 4% polyacrylamide gels in 0.25 M Tris-borate ethylenediaminetetraacetate (EDTA) buffer at 120 mV for 2 h. The gel was then dried and subjected to autoradiography at room temperature.

Northern blotting

Total cellular RNA was isolated from the cells using a TRizol Reagent (Invitrogen). The oligonucleotide primers specific for human *COX-2* (5′-TTCAAAT GAGATTGTGGGAAAATTGCT-3′; 5′-AGATCAT CTCTGCCTGAGTATCTT-3′) were used for amplification of a 305-base pair (bp) fragment of the human *COX-2* mRNA. Twenty micrograms of total cellular RNA per lane were electrophoresed in a formaldehyde-containing 1.2% agarose gel and transferred to nylon-supported membranes. After cross-linking, membranes were prehybridized overnight in a solution containing 50% formamide, 5× sodium chloride/sodium phosphate/EDTA buffer, 5× Denhardt's solution, 0.1% sodium dodecyl sulfate (SDS), and 100 µg/ml single-stranded salmon sperm DNA, and then hybridized for 12 h at 42°C with radiolabeled cDNA probes for the human COX-2 probe, which was labeled with [a-^{32}P]dCTP by random priming. After hybridization, membranes were washed twice for 10 min at 42°C in 0.1× standard saline citrate and 1% SDS twice for 10 min in the same solution at 42°C, and exposed to an X-ray film at −80°C for 5–7 days.

Western blotting

Total protein extracts from the HCT116 cell line were solubilized by a sample buffer (2% SDS, 125 mmol/l Tris-HCl, pH 7.4, 20% glycerol, and 2% 2-mercaptoethanol) at room temperature for 5 min and applied onto a 10% SDS polyacrylamide gel. After electrophoresis, proteins were transferred to polyvinylidene difluoride membranes (Bio-Rad, Richmond, VA, USA). The blots were blocked with 5% nonfat dry milk in PBS with 0.1% Tween20 for 1 h at 4°C and incubated with affinity-purified anti-PPARα antibody (1 µg/ml) overnight at 4°C. The blots were then incubated with the anti-mouse immunoglobulin conjugated with horseradish peroxidase (sc-2005) (Santa Cruz Biotechnology) for 1 h at 4°C. An enhanced chemiluminescence kit (Amersham Pharmacia Biotech, Buckinghamshire, UK) was used for detection.

Transfection of siRNA

The TransSilent PPARα small interfering RNA (siRNA) vector and TransSilent Control vector were purchased from Panomics (Redwood, CA, USA). Five micrograms of the PPARα siRNA vector or control siRNA vector were cotransfected with luciferase vectors. Luciferase activities were assayed and quantified according to the same methods described above.

Statistics

Comparisons between groups were made with Student's *t* test. A difference between groups of $P < 0.05$ was considered significant.

Results

Effects of bile acids on the transcriptional activity of the COX-2 *gene*

To investigate the ability of the bile acids to modulate the expression of *COX-2*, transient transfections were performed with the *COX-2* promoter–luciferase construct (−1555/+178) into HCT116 or HT29 cells. As is evident from Fig. 1A, in HCT116 cells, treatment with 200 µM LCA caused an 8.2-fold increase in luciferase activity compared with the control; 200 µM DCA caused a 7.3-fold increase and 200 µM CDCA caused a 5.0-fold increase in luciferase activity compared with the control. In contrast, taurocholic acid (TCA), cholic acid (CA), and conjugated bile acids did not cause any change in the rate of *COX-2* transcription (Fig. 1A). Similar results were observed in HT29 cells. The addition of 200 µM LCA caused a 5.5-fold increase in HT-29 cells (Fig. 1B). *COX-2* transcription by LCA in HCT116 cells

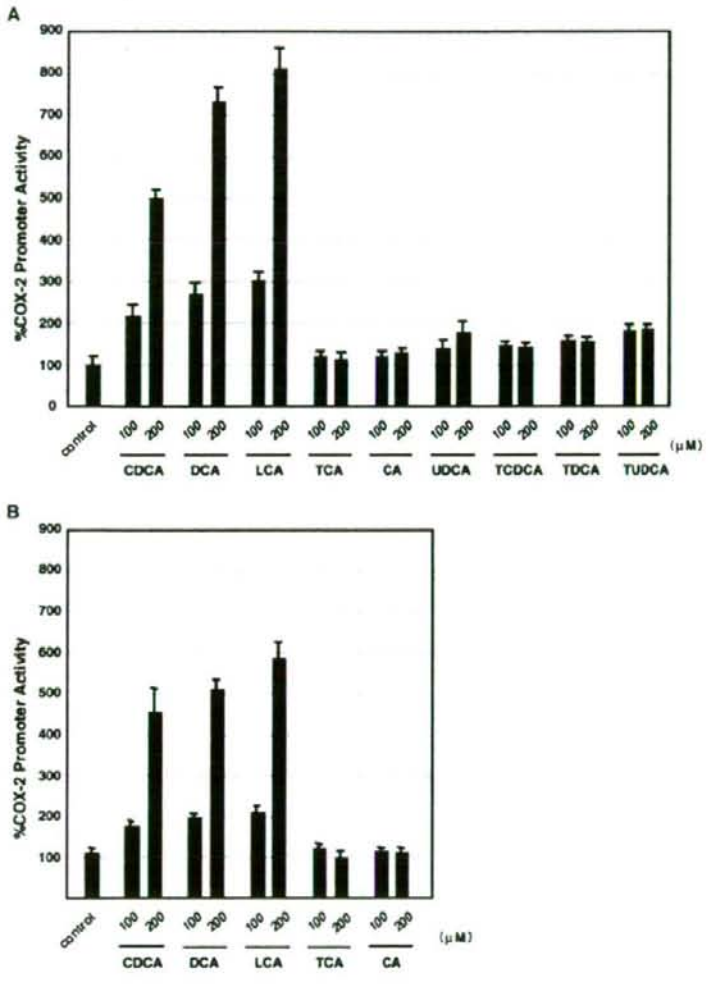

Fig. 1A, B. Cyclooxygenase-2 (*COX-2*) promoter assays for various bile acids. To test the effect of bile acids on the transcription of the *COX-2* gene, the luciferase reporter plasmid containing the COX-2 promoter (−1555/+178) was transferred into the HCT116 cells (A) or HT29 cells (B) with 100 or 200 μM of chenodeoxycholic acid (*CDCA*), deoxycholic acid (*DCA*), lithocholic acid (*LCA*), taurocholic acid (*TCA*), cholic acid (*CA*), ursodeoxycholic acid (*UDCA*), taurochenodeoxycholic acid (*TCDCA*), taurodeoxycholic acid (*TDCA*), or tauroursodeoxycholic acid (*TUDCA*). UDCA, TCDCA, TDCA, and TUDCA were tested only in HCT116 cells. The COX-2 promoter activities were measured in the cellular extracts 24 h later. *Columns*, means; *bars*, SD; $n = 4$

was dose dependent (Fig. 2A). To confirm the transcriptional activation of the *COX-2* gene, we analyzed the expression of *COX-2* mRNA by Northern blot analysis and observed a positive correlation between the concentration of LCA (0–200 μM) and the amount of the *COX-2* mRNA (Fig. 2B).

Localization of the region of the COX-2 *promoter that mediates the effects of LCA*

To understand what response elements in the *COX-2* promoter are involved in LCA-induced transcriptional activation, transient transfections were performed using various deletion constructs of the *COX-2* promoter. As shown in Fig. 3B, LCA treatment induced *COX-2* promoter (−1555/+178) activity that was increased 8.2-fold compared with that of LCA-untreated cells of the same construct (control). The luciferase activities of the deleted constructs, −894/+178, −423/+178, and −240/+178, were of almost the same magnitude. A slight reduction in the response was observed with the (−139/+178) construct. The shortest construct (−44/+178) lacking all response elements showed no induction compared with the LCA-untreated cells (control). These data suggest that transcriptional activator elements between −240 bp and −44 bp may be responsible for mediating the effects of LCA (Fig. 3B). In the 240-bp region upstream of the transcriptional start site, potential binding sites for

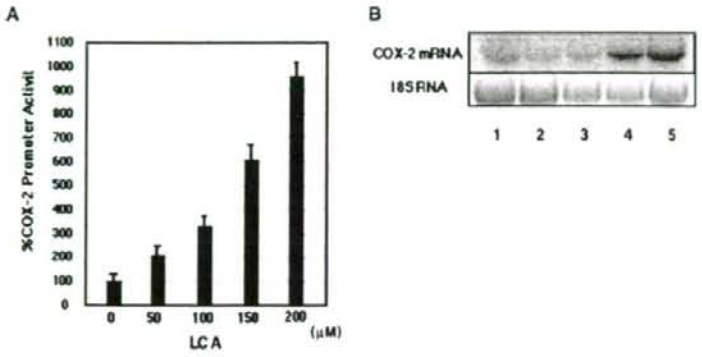

Fig. 2A, B. The effect of LCA on *COX-2* gene expression. **A** *COX-2* promoter assays with the various concentrations of LCA. *Columns*, means; *bars*, SD; $n = 4$. **B** Northern blot analysis of the *COX-2* mRNA. *Lane 1*, not treated with LCA; *lane 2*, LCA 50 μM; *lane 3*, LCA 100 μM; *lane 4*, LCA 150 μM; *lane 5*, LCA 200 μM. RNA was extracted from cells treated with LCA for 24 h

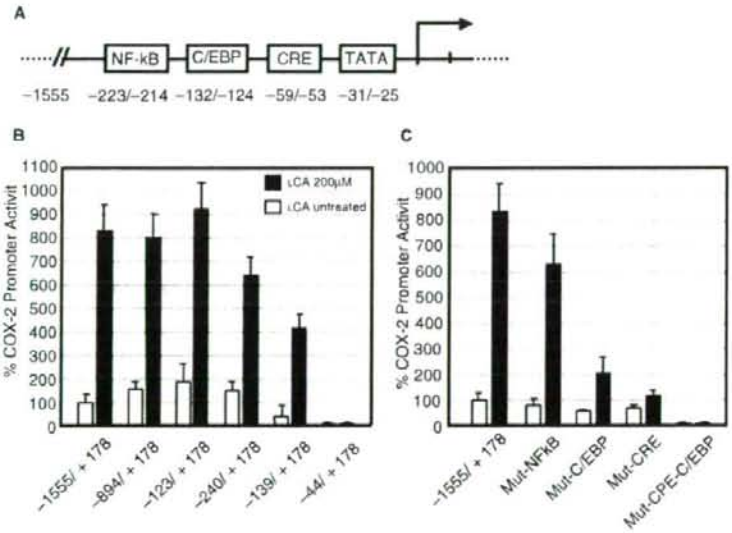

Fig. 3A–C. To elucidate the main transactivation domain induced by LCA in the *COX-2* promoter, promoter assays were carried out by exposing different mutants to LCA. **A** At 200 bp upstream of the TATA box, potential binding sites for transcription factors were identified, including a nuclear factor κB (*NF-κB*) binding site, C/EBP binding site, and a cyclic AMP response element (*CRE*) site. **B** Three micrograms of deletion mutants of *COX-2* promoter (−1555/+178, −894/+178, −423/+178, −240/+178, −139/+178, and −44/+178) and 20 ng of pRL-TK were transiently transfected into HCT116 cells with 200 μM LCA (*black columns*) or without LCA (*open columns*) for 24 h, and then the luciferase activity was measured. *Columns*, means; *bars*, SD; $n = 4$. **C** Three micrograms of mutant constructs of the *COX-2* promoter and 20 ng of pRL-TK were transiently transfected into HCT116 cells and exposed to LCA 200 μM (*black columns*) or vehicles (*open columns*) for 24 h. *Mut-NFkB*, the −1555/+178 COX-2 plasmid with a mutation in the NF-κB site, *Mut-C/EBP*, the −1555/+178 COX-2 plasmid with a mutation in the C/EBP site, and *Mut-CRE*, the −1555/+178 COX-2 plasmid with a mutation in the CRE site were used. *Columns*, means; *bars*, SD; $n = 4$

transcriptional factors were identified including an NF-κB site (−223/−214), a C/EBP site (−132/−124), a CRE site (−59/−53), and a TATA site (−31/−25) (Fig. 3A).

Site-directed mutation analysis of the COX-2 *promoter*

To analyze the precise mechanism of the transcriptional activation by LCA, transfection analyses were performed using *COX-2* promoter constructs in which specific binding sites were destroyed by site-directed mutagenesis (Table 1). As shown in Fig. 3C, mutations of the CRE and C/EBP sites caused a significant decrease in the response to 200 μM LCA compared with LCA-untreated cells (control). By contrast, mutation of the NF-κB site had little effect on the *COX-2* promoter activity. In addition, the construct with the

double mutation of C/EBP and CRE showed no luciferase activity either with or without LCA (Fig. 3C).

Adenovirus-mediated expression of LST-2 activates bile acid-mediated induction of the COX-2 *gene in HepG2 cells*

The present overexpression system using an adenovirus carrying the *LST-2* gene would be useful for detailed characterization of LST-2 functions. The Northern blot analysis previously performed revealed that LST-2 was not expressed in HepG2 cells.[1] To investigate the functional role of LST-2 in *COX-2* transcriptional activation, we infected HepG2cells 24 h previously with adenovirus carrying the *LST-2/OATP8/OATP1B3* gene or *b-gal* gene (control), and then measured the luciferase activity of the transfection with the *COX-2* promoter–luciferase construct (−1555/+178) into the cells followed by addition of 200 μM bile acids for 24 h. CDCA, DCA, and LCA resulted, respectively, in 2.4, 3.2, and 4.1-fold increases in luciferase activity compared with the control (Fig. 4). In contrast, neither TCA nor CA caused any change in the luciferase activity. These data suggest that the expression of LST-2 plays an important role in activating the *COX-2* promoter induced by these bile acids in HepG2 cells.

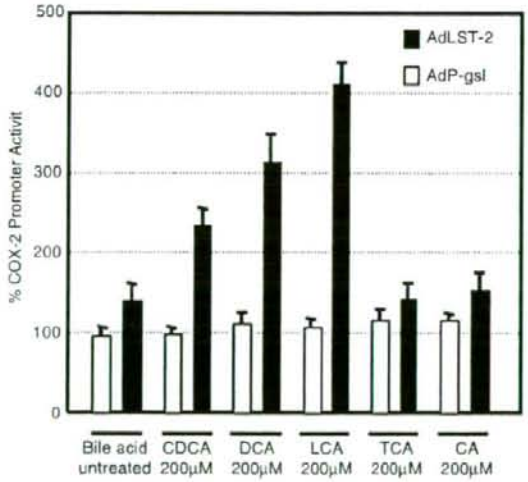

Fig. 4. LST-2/OATP8/OATP1B3 was involved in bile acid-induced COX-2 expression. HepG2 cells were infected with *AdLST-2* (30 pfu/cell) and incubated for 24 h, and then transient transfections were performed with 0.75 μg of the human *COX-2* promoter–luciferase construct (−1555/+178) and 5 ng pRL-TK. Following transfections, cells were treated with 200 μM CDCA, DCA, LCA, TCA, or CA for 24 h, and then luciferase activities were measured. Luciferase activities in the *AdLST-2* infected cells are shown (*black columns*). *Adb-gal* infected cells were used as a control (*open columns*). *Columns*, means; *bars*, S.D.; $n = 4$

Electrophoretic mobility shift assay of the COX-2 *promoter*

Electrophoresis mobility shift assays (EMSAs) were performed to identify the transcription factor that mediated the induction of *COX-2* by LCA. A positive correlation was observed between the concentration of LCA and the amount of DNA binding protein binding to the CRE site of the *COX-2* promoter (Fig. 5A, lanes 2–6). In contrast, C/EBP binding sites showed no significant correlation between the amount of the DNA binding protein binding to the C/EBP site and the concentration of LCA (Fig. 5B, lane 2–6). Addition of a specific antibody against PPARα and CREB revealed that formation of the specific protein–DNA complex was inhibited (Fig. 5C, lanes 9 and 15). In contrast, protein–DNA complex formation in LCA-untreated nuclear extract was not inhibited by addition of PPARα antibody (Fig. 5C, lane 17). These results suggest that PPARα and CREB are constituents of the protein–DNA complex bound to the CRE site and that this specific protein–DNA complex is dependent on the concentration of LCA. Neither PPARβ, PPARγ, PPARδ, AP-1, nor c-Fos resulted in any change in the DNA binding complex (Fig. 5C, lanes 10–15).

PPARα-specific agonist increases the transcriptional activity of the COX-2 *gene*

To examine whether PPARα could regulate the *COX-2* gene at the transcriptional level, luciferase analysis was performed, followed by various concentrations of WY14643, which is a PPARα-specific agonist. The addition of 100 μM WY14643 caused a 5.6-fold increase in luciferase activity compared with WY14643-untreated cells (Fig. 6A), and the mutant construct of the *COX-2* promoter (−1555/+178; Mut-CRE) showed no change in luciferase activity (Fig. 6B). In contrast, the PPARβ/δ agonist GW501516 and the PPARγ agonist ciglitazone showed no effect on the transcriptional activity of the *COX-2* gene (Fig. 6C, D). These results indicated that activation of the *COX-2* gene at the CRE site is specific for PPARα.

Specific downregulation of PPARα *mRNA inhibits LCA-mediated induction of* COX-2

Whereas the above results strongly suggest that PPARα is a key molecule in the LCA-mediated induction of *COX-2*, we next sought to confirm the depletion of the PPARα. In mammalian cells, siRNA technology allows the targeted degradation of specific mRNA molecules,

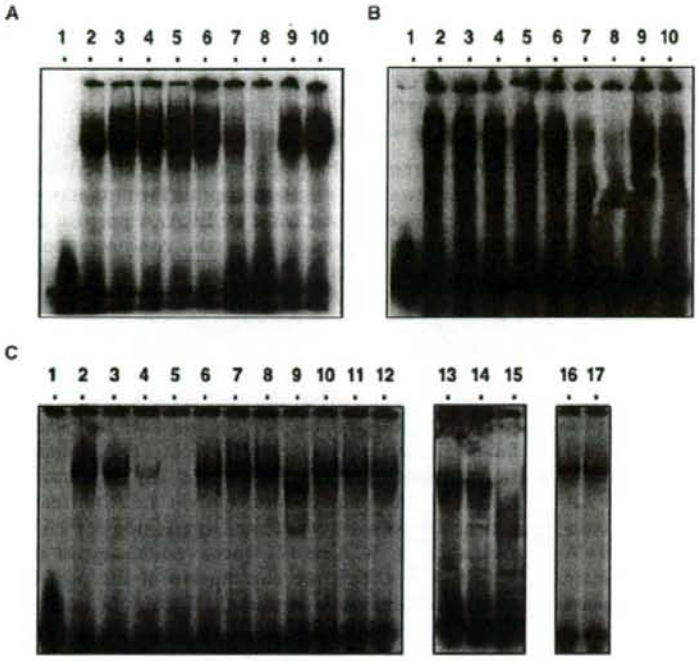

Fig. 5A–C. Electrophoretic mobility shift assays (EMSAs) for the identification of the transcription factor in the LCA-dependent induction of the *COX-2* gene. **A, B** EMSA was carried out using oligonucleotides of CRE (**A**) or C/EBP (**B**) and 20 μg of nuclear protein from HCT116 cells. Free probe (*lane 1*); untreated with LCA (*lane 2*); LCA (50, 100, 150, or 200 μM, lanes 3–6); 200 μM LCA plus cold competitor (10×, 100×, *lanes 7* and *8*); 200 μM LCA plus mutant competitor (10×, 100×, *lanes 9* and *10*). **C** Addition of a specific antibody against peroxisome proliferator-activated receptor (PPAR) α, PPARβ, PPARγ, PPARδ, CRE binding protein (CREB), activator protein 1 (AP-1), and c-Fos. EMSA was carried out using oligonucleotides of CRE and 20 μg of nuclear protein from HCT116 cells. Free probe without nuclear extract (*lane 1*); 200 μM LCA (*lane 2*); 200 μM LCA plus cold competitor (1×, 10×, 100×, *lanes 3–5*); 200 μM LCA plus mutant competitor (1×, 10×, 100×, *lanes 6–8*). *Lanes 9–15* show nuclear extract from LCA (200 μM)-treated cells incubated with antibodies to PPARα (*lane 9*), PPARβ (*lane 10*), PPARγ (*lane 11*) and PPARδ (*lane 12*), AP-1 (*lane 13*), c-Fos (*lane 14*), and CREB-1 (*lane 15*). The addition of the specific antibody for PPARα and CREB resulted in a supershift band. A faint band was observed using nuclear extract from LCA-untreated HCT116 cells (*lane 16*). However, there was no change with the LCA-untreated nuclear extract plus PPARα antibody (*lane 17*)

thus inhibiting the expression of the corresponding genes in the cells.[42] When cotransfections were performed with the *COX-2* promoter–luciferase construct (−1555/+178) and the TransSilent PPARα siRNA vector transfected into HCT116 cells followed by 200 μM LCA for 24 h, the TransSilent PPARα siRNA vector suppressed the LCA-mediated induction of *COX-2* compared with control vector cotransfection (Fig. 7B).

Discussion

Bile acids are known as endogenous promoters of gastrointestinal cancers,[24,25] and overexpression of COX-2 contributes to colorectal carcinogenesis. Hence, it is important to determine whether endogenous inducers of COX-2 contribute to carcinogenesis.[16,43] Our previous work provided evidence that the bile acid transporter LST-2 is weakly expressed in the normal human liver but strongly expressed in gastrointestinal cancers, suggesting that it plays an important role in the uptake of bile acids even in gastrointestinal cancer cells.[1] Until now, the precise mechanisms by which LST-2 is expressed in gastrointestinal cancers were not known. Luminal contents, including bile acids, have been reported to induce the overexpression of COX-2.[44] Therefore, it is possible that bile acid transported by LST-2 in colonic cancer cells may also influence carcinogenesis in the colon. In this paper, we studied the molecular mechanisms by which bile acids induce the transcription of *COX-2*, and the role of LST-2 in the colonic cell lines HCT116 and HT29.